Nanoscale

PAPER

View Article Online
View Journal

Cite this: DOI: 10.1039/c7nr08529j

Numerical insights into the early stages of nanoscale electrodeposition: nanocluster surface diffusion and aggregative growth†

Mesfin Haile Mamme, *[a,b] Christoph Köhn, [a,c] Johan Deconinck [b] and Jon Ustarroz *[a]

Fundamental understanding of the early stages of electrodeposition at the nanoscale is key to address the challenges in a wide range of applications. Despite having been studied for decades, a comprehensive understanding of the whole process is still out of reach. In this work, we introduce a novel modelling approach that couples a finite element method (FEM) with a random walk algorithm, to study the early stages of nanocluster formation, aggregation and growth, during electrochemical deposition. This approach takes into account not only electrochemical kinetics and transport of active species, but also the surface diffusion and aggregation of adatoms and small nanoclusters. The simulation results reveal that the relative surface mobility of the nanoclusters compared to that of the adatoms plays a crucial role in the early growth stages. The number of clusters, their size and their size dispersion are influenced more significantly by nanocluster mobility than by the applied overpotential itself. Increasing the overpotential results in shorter induction times and leads to aggregation prevalence at shorter times. A higher mobility results in longer induction times, a delayed transition from nucleation to aggregation prevalence, and as a consequence, a larger surface coverage of smaller clusters with a smaller size dispersion. As a consequence, it is shown that a classical first-order nucleation kinetics equation cannot describe the evolution of the number of clusters with time, $N(t)$, in potentiostatic electrodeposition. Instead, a more accurate representation of $N(t)$ is provided. We show that an evaluation of $N(t)$, which neglects the effect of nanocluster mobility and aggregation, can induce errors of several orders of magnitude in the determination of nucleation rate constants. These findings are extremely important towards evaluating the elementary electrodeposition processes, considering not only adatoms, but also nanoclusters as building blocks.

Received 15th November 2017,
Accepted 8th March 2018

DOI: 10.1039/c7nr08529j

rsc.li/nanoscale

1 Introduction

Electrochemical deposition is, since the 19th century, a core technology for many industrial applications.[1,2] During the last decades, this technique has also been successfully employed for the preparation of a wide variety of supported nanostructured materials[3] (nanoparticle distributions, thin films, *etc*.) with applications in many fields, ranging from (bio) sensing[4–7] to catalysis.[8–11] When compared to other synthesis methods in the liquid or gas phase, electrochemical deposition offers several advantages such as allowing the nucleation and growth of the new phase directly on the substrate of interest. Moreover, the physico-chemical and structural properties of the deposited material can be tuned by the interplay of applied potentials, electrolyte composition, substrate-electrolyte-growing phase interactions, *etc*. Although the interplay of such different phenomena provides interesting pathways to achieve a good control of the morphology and structure of the deposited material in the nanoscale, it also adds complexity to the fundamental understanding of each elementary step taking place during the electrodeposition process, especially during its initial stages.

The early stages of electrochemical nucleation and growth have been exhaustively studied for decades,[12] resulting in a classic nucleation and growth theory which is based on the assumption that, once stable nuclei are formed, growth occurs by atomic addition until the reaction is halted (*i.e.*, atoms are the only building blocks in the process). It can be summarized

---

[a] *Vrije Universiteit Brussel (VUB), Research Group Electrochemical and Surface Engineering (SURF), Pleinlaan 2, 1050 Brussels, Belgium. E-mail: jon.ustarroz@vub.be*

[b] *Vrije Universiteit Brussel (VUB), Department of Electrical Engineering and Power Electronics, Pleinlaan 2, 1050 Brussels, Belgium. E-mail: mmamme@vub.be, mesfin.mekdi@gmail.com*

[c] *DTU Space, National Space Institute, Technical University of Denmark, Elektrovej 328, 2800 Lyngby, Denmark*

† Electronic supplementary information (ESI) available. See DOI: 10.1039/C7NR08529J

as follows: first, when the applied potential is negative enough to force the reaction $Me^{z+} + ze^- \rightarrow Me(s)$, metal cations are electrochemically reduced to metal adatoms at the interface between the substrate and the electrolyte. As a consequence, new interfaces are created, with a concomitant increase of the free Gibbs energy of the system. Due to this excess energy, the metal adatoms diffuse randomly (Brownian motion) on the surface of the electrode depending on the metal–substrate interactions. During this time, diffusing adatoms may encounter other adatoms, atomic clusters or surface defects. This results in the locking of adatoms (or clusters) to surface defects, or the aggregation of several atoms, since both processes reduce excess surface energy generated by the deposited foreign phase. Eventually, upon reaching a critical size (or locking to a surface defect), the thermodynamic formation energy of the clusters is larger than their surface energy. Thereafter, such a cluster can be considered a stable nucleus, which grows irreversibly by the incorporation of more atoms until the electrochemical reduction is no longer thermodynamically favourable (*i.e.*, a negative potential is no longer applied).

Depending on the interactions between the metal and the substrate, three different growth modes are generally accepted. In this work, we focus on the case in which the deposited metal atoms are more tightly bound to each other than to the substrate. Hence, the nuclei adopt the shape of hemispherical islands which grow radially by the so-called Volmer–Weber 3D island growth mechanism.[12] This is the case of metals on carbonaceous materials such as glassy carbon or graphite, which results in the electrodeposition of nanoparticle distributions, commonly used for electrocatalytic or sensing applications.[13,14]

In the early stages, two growth processes have been traditionally considered. First, a metal ion can be discharged into an adatom on an arbitrary site of the electrode surface and can migrate randomly on the surface until it is incorporated into a nucleus. Second, the electrochemical reduction of a metallic cation can take place on the surface of the growing nucleus directly. In general, the contribution of atomic surface diffusion has been neglected and direct reduction of metallic ions onto growing nuclei is considered as the only mechanism involved in electrochemical growth. Such a mechanism is henceforth referred to as direct attachment.[1,3,12,15–17] Based on these assumptions, and considering first-order nucleation kinetics,[18] analytical formulations of the current (I–t) transients obtained upon the application of a constant potential (potentiostatic electrodeposition) have been developed through several decades. These give rise to several well-established models for the 3D growth of multiple nuclei under diffusion control: Scharifker–Hills (SH),[19] Scharifker–Mostany (SM),[20] Mirkin and Nilov (MN),[21] and Heerman and Tarallo (HT)[22] among others.[15,23–25] Further mathematical developments have completed these models by adding co-deposition reactions[26,27] or mixed and kinetic control.[28,29]

By fitting these analytical models to the experimental I–t transients, the evolution of the number of nuclei with time, $N(t)$, can be inferred. Interestingly, the comparison of $N(t)$ inferred from modelling I–t transients and $N(t)$ calculated after physical characterization of nuclei grown for different times leads to a large controversy over the correctness and applicability of such models. In some cases, a good agreement is found,[30–33] whereas, in other cases, nucleation rates obtained from the analytical model can differ up to five orders of magnitude from those obtained using experimental imaging techniques.[16,18,34–38] It is worth re-emphasizing here that, in spite of different mathematical formulations, all the models cited previously are based on the growth of all stable nuclei being only mediated by direct attachment.

Over the last decades, the improvement of characterization techniques has allowed the community to investigate electrochemical nucleation and growth phenomena with higher resolution by *ex situ*[36,39] and *in situ*[18] transmission electron microscopy (TEM). Very recently, non-contact lateral molecular force microscopy employing vertically oriented probes has been used with unprecedented spatiotemporal resolution to probe *in situ*, the dynamic processes occurring during the early stages of metal nucleation.[40] Also, the use of nanoelectrodes[41,42] or scanning electrochemical cell microscopy (SECCM)[38,43] has allowed one to probe electrochemical nucleation phenomena in ultra-small surfaces, giving rise to the possibility of detecting current spikes which arise from the growth of single nuclei. Based on the combination of these characterization techniques, several novel phenomena, which are not accounted for within the classical theory of nucleation and growth, have been reported. For instance, nanocluster detachment from the substrate,[38,43] secondary nucleation,[44] self-terminated growth,[45,46] nanocluster surface movement, aggregation and coalescence[36–38,40,43,47] have been found to highly influence the early stages of nucleation and growth. Unfortunately, these processes cannot be described by the analytical models mentioned previously.

Due to the high level of complexity of the process and the small timescales and lengthscales which need to be considered, electrochemical and surface characterization techniques feature inherent limitations. Electrochemical measurements suffer from poor signal-to-noise ratio, whereas *in situ* TEM characterization may lack surface sensitivity or spatial resolution and only offers limited data interpretation and reproducibility due to the strong interaction of the electron beam with the electrolyte and electrode material.[48] Therefore, a complementary approach based on numerical simulations is highly sought after.

During the last decades, different models have been built to describe and simulate numerically the early stages of heterogeneous nucleation and thin-film growth for different experimental processes, such as chemical vapor deposition (CVD),[49] physical vapor deposition (PVD),[50,51] molecular beam epitaxy (MBE),[50,52] low energy cluster beam deposition (LECBD)[50,52] and other techniques.[51] Some of the most well-established models are the percolation model (PM),[53] the diffusion limited aggregation (DLA) model,[54] the cluster–cluster aggregation (CCA) model[50] and the deposition diffusion aggregation (DDA) model.[50–52] In brief, the PM model only considers the influx of atoms into the substrate but neglects the surface diffusion of adatoms and clusters. In the DLA model, the surface diffusion and aggregation of adatoms are incorporated whereas, in the CCA model, the surface diffusion and aggregation of clusters are also taken into consideration. However, both DLA and CCA models do not take into account a continuous influx of new atoms into the substrate. Alternatively, the DDA model considers explicitly continuous deposition and the diffusion and aggregation of both adatoms and clusters.

In comparison with non-electrochemical processes, fewer attempts have been made to model, numerically, the early stages of thin-film/island growth during electrochemical deposition. For example, the case of 3D-diffussion controlled growth was studied by the boundary element method.[55,56] Besides, the cause of particle size dispersion assuming instantaneous nucleation followed by diffusion controlled growth was modelled using Brownian dynamics.[57] It was found that particle dispersion is linked to the heterogeneous distribution of the inter-particle distance. Similar studies were also conducted by introducing two parameters: a reaction distance parameter to correct the discretization error and the environmental potential parameter to analyze the influences of the size and growth of a nucleus on its surrounding.[58] Furthermore, a kinetic Monte Carlo (KMC) model was developed to study the effects of the metal–substrate surface diffusion energy barrier and the kinetics of attachment of adatoms during the initial stages of electrodeposition at low overpotential. The simulation showed that a higher cluster density is achieved when the metal-on-substrate surface diffusion is low compared with the metal-on-metal surface diffusion.[59] Later, the same approach was used to simulate the growth of predefined seeds on the substrate[60] leading to the conclusion that more uniform size distributions are possible by increasing the number of seeds. Furthermore, the formation of surface alloys in the early stages of electrochemical deposition has also been studied by coupling microcanonical molecular dynamics (MMD) and BD models[61,62] making possible to discern between layer-by-layer growth for Ag on Au(111) and surface alloy formation for the case of Pt on Au(111).

It is worth reemphasizing here that all the electrochemical growth models are based on the assumption that atoms are the only building blocks during the early stages of electrochemical nucleation and growth (growth is only mediated by direct attachment) and that, as a consequence, the surface diffusion and aggregation of nanoclusters are neglected. Besides, the current models are applicable only under previously specified nucleation modes (instantaneous and/or progressive) and growth modes (kinetics or diffusion controlled).[55,56]

In this work, we elaborate a novel modelling approach that combines a finite element method (FEM) with random walk simulations. The FEM[63] provides the surface concentration and the net flux of adatoms discharged on the surface based on the applied potential, whereas the random walk algorithm is used to simulate the surface diffusion and aggregation of adatoms and clusters. By using this tool, we provide significant evidence that supports the recent experimental findings on an electrochemical aggregative growth mechanism during the initial stages of nanoscale electrodeposition.[36,37,43] To the best of our knowledge, we introduce for the first time the concept of cluster diffusion and aggregation, during continuous deposition in one nanoscale electrodeposition model.

2 Model description

In this section, we define the terms used throughout this paper and discuss the model assumptions in detail. *Adatoms* are isolated metal atoms that are formed after the electrochemical reduction of metal cations on the substrate. *Clusters and adatom-aggregates* are groups of adatoms connected together irreversibly. We use the term cluster when its radius is larger than a certain arbitrary threshold and the term adatom-aggregate when its radius is smaller. *Aggregates* are groups of two or more clusters connected together irreversibly. Note that the term *particles* is used to refer to adatoms, clusters and aggregates together. Finally, we define *induction time* as the time that is needed for the first cluster larger than a given size to be formed.

2.1 Deposition model and assumptions

In this work, the continuous deposition of metal adatoms on the surface is modelled by using a time dependent multi-ion transport and reaction model (TD-MITReM).[63,64] The TD-MITReM is used to solve the mass balance equation of all the species and electrolyte potential in each time step. This model takes into account the transport driven by convection, migration and diffusion of all relevant species in the electrolyte, together with homogeneous reactions in the electrolyte and electrochemical reactions at the electrode.[63,65] The solution of this model results in a time dependent current density produced by the electrochemical reduction of metal cations on the surface. In this work, we use the electrochemical reduction of silver from an acetonitrile solution containing 1 mM $AgNO_3$ and 0.1 M $LiClO_4$ as a case study. In this way, the following assumptions can be made: the electrochemical reaction consists of only one-step reduction ($Me^+ + 1e^- \rightarrow Me_{ads}$) and no homogeneous reactions occur in the electrolyte. The kinetics of the electrochemical reaction was modelled with the Tafel equation[63,65] and all simulations were carried out far from the equilibrium potentials, so underpotential deposition and anodic dissolution can be neglected.

Fig. 1(a) shows the current density obtained after the application of various electrode potentials ($E = -0.11$ to $E = -0.3$ V *vs.* the SHE, corresponding to overpotentials $\eta = 560$ mV to $\eta = 750$ mV). By using Faraday's law, the resulting current density is transferred to the surface diffusion model as an *influx* of metal adatoms at random locations on the electrode surface. For simplicity, the different influxes are referred hereafter to as influx factors, F, by normalizing them to the influx obtained for the lowest simulated overpotential, $\eta = 560$ mV. Here, the following remark must be borne in mind. The way in which the overpotential translates into an influx of adatoms depends

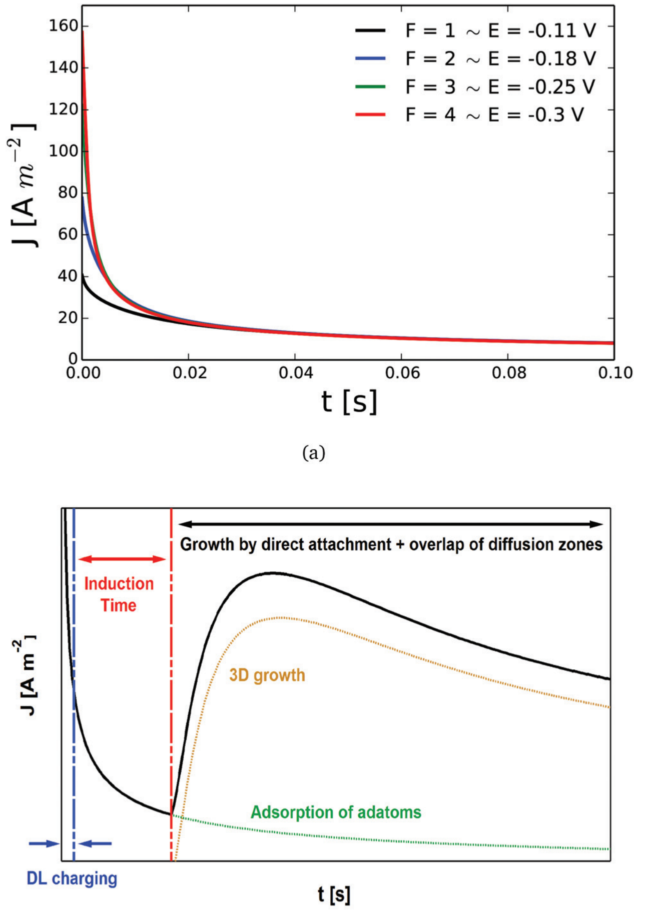

(a)

(b)

Fig. 1 (a) Current–time transients obtained from the FEM simulation of the electrochemical reduction of silver at different overpotentials. The solution contained 1 mM $AgNO_3$ and 0.1 M $LiClO_4$ as a supporting electrolyte in an acetonitrile solution. (b) Schematics of a typical chronoamperometric current transient obtained during an electrodeposition experiment following a potential step.

not only on the overpotential (reaction kinetics) but also on the mass transport conditions: diffusion, migration and convection. Since the mass transport conditions are the same in all the simulations, each influx of adatoms is directly related to a given overpotential and therefore, we use the terms *influx* and *overpotential* indistinctly in this article. However, if mass transport conditions were different, each overpotential will lead to a different influx.

It must be noted that the current–time transients shown in Fig. 1(a) do not display the characteristic peaked shape, typical of electrochemical growth of 3D islands under diffusion control.[20,66] Instead, the simulated transient displays a monotonically decreasing current profile. The reason is that, during the initial stages, prior to the formation of stable nuclei, electrodeposition proceeds by the discharge of metal adatoms on the substrate and the formation of sub-critical clusters.[32,36,37] During this initial time, defined as induction time in several occasions,[24,25,36–38,41,67] the active surface area has not started to increase yet by the formation of growing active nuclei. Instead, a characteristic $I \propto t^{-1/2}$ relationship (Cotrellian behaviour), typical of electrochemical reactions occurring on a non-growing surface under planar diffusion limitations, is expected.[68] Fig. 1(b) shows a scheme exemplifying the different time-domains of a potentiostatic electrodeposition current–time transient.[18,27,36,37,69,70] At short times, the current transient decays monotonically due to the electrical double layer charging (DL charging) and due to the formation of sub-critical clusters (induction time). At longer times, the current increases due to three-dimensional growth by direct attachment and presents a maximum due to the overlapping of diffusion zones. The transient ends up decaying at $I \propto t^{-1/2}$, typical of linear diffusion. The transients simulated in Fig. 1(a) correspond to the region at the left of the red line (induction time) of Fig. 1(b).

2.2 Surface diffusion model and assumptions

The physico-chemical interactions between the deposited metal and the substrate have been extensively studied and have been shown to have a strong effect on the electrochemical nucleation and growth process. Hence, different metal nanostructures, size distributions and morphologies are obtained for different combinations of the deposited metal and substrate materials.[36–38,71–77] It is crucial to emphasize that the surface diffusion, not only of adatoms, but also of small nanoclusters (NCs) must be considered, since it has been shown that clusters as large as a few nanometers in diameter are mobile when supported on carbon[36,37,47,78,79] or ITO[40] substrates in an electrochemical environment.

The *surface diffusion/mobility* is the direct result of the surface energy difference between the metal adatoms and/or clusters and the electrode material. In other words, when the binding energy between deposited species and the substrate becomes lower, the surface tension becomes higher, and the surface diffusion is enhanced. Therefore, the adatoms, but also the small clusters, move randomly along the surface of the electrode. To minimize excess surface energy, adatoms and clusters aggregate with each other. The surface diffusion decreases with an increase of the cluster size.[50–52,59,80] Several mathematical models have been postulated[50,59,79] and the surface diffusion coefficient, D [m^2 s^{-1}], of a cluster can be defined as

$$D = D_0 \cdot N_{\text{adatoms}}{}^{-\alpha} \tag{1}$$

where D_0 [m^2 s^{-1}] is the surface diffusion coefficient of an adatom ($D_0 = 2 \times 10^{-9}$ m^2 s^{-1})[81] with N_{adatoms} being the number of adatoms forming the cluster. α represents the relative mobility of small and large clusters ($\alpha \geq 0$). Hereafter, α is referred to as the relative surface mobility factor.

Fig. 2 shows the dependence of the cluster diffusion coefficient as a function of the cluster size for different values of α. Larger values of α result in a sharper drop in the surface diffusion coefficient with increasing cluster size. This means that the assumption that only single adatoms diffuse on the substrate during the initial stages of electrodeposition would

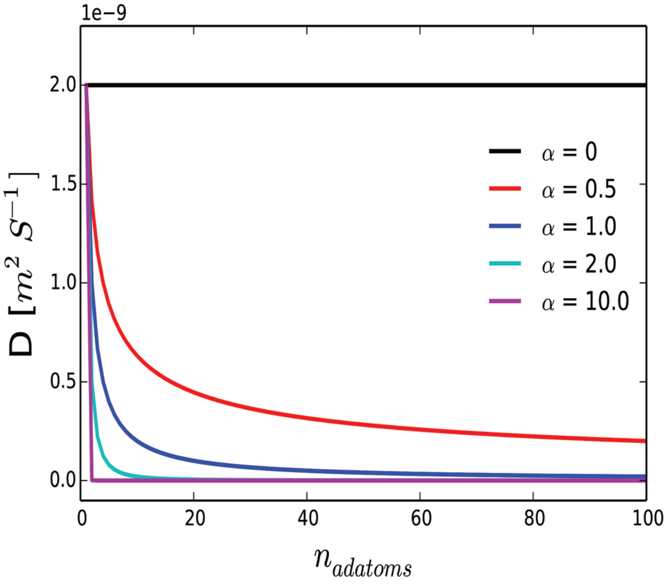

Fig. 2 Cluster surface diffusion as a function of the number of adatoms within a cluster for different relative surface mobility factors, α.

only be acceptable for large values of α (typically 10). Contrarily, for small α ($\alpha \approx 0.5$), the surface diffusion coefficient of nanoclusters of up to hundreds and thousands of atoms ($r \approx 1$–1.5 nm) cannot be neglected. The same power law has been adopted by Jensen *et al.*[50–52] to study surface diffusion and aggregation during the growth of thin films in non-electrochemical processes.

We model the motion of individual metal particles (adatoms and clusters) as spheres with different radii R_i and masses m_i on a 300 × 300 nm^2 surface under periodic boundary conditions. At every time step the center $\mathbf{r}$ of each particle is updated through[57]

$$\mathbf{r}(t_{n+1}) = \mathbf{r}(t_n) + 2\sqrt{D\Delta t}\cdot\mathcal{R}\cdot\begin{pmatrix}\cos(\varphi_R)\\ \sin(\varphi_R)\end{pmatrix} \tag{2}$$

where $\mathcal{R} = \sqrt{-2\ln(\mathcal{N}_1)}$ as well as $\varphi_R = 2\pi\mathcal{N}_2$ with uniform random numbers $\mathcal{N}_i \in [0,\ 1)$. For all the simulations we choose $\Delta t = 1$ ns. After every time step, the collision of metal particles with indices i and j is checked and evaluated by the condition

$$\sqrt{(x_i - x_j)^2 + (y_i - y_j)^2} \le R_i + R_j\ \forall i,j \tag{3}$$

where x_i and y_i are the components of $\mathbf{r}_i$. If two metal particles collide, the mass and volume of both particles are added, hence $R_{\text{new}} = \sqrt[3]{R_i^3 + R_j^3}$ and $m_{\text{new}} = m_i + m_j$; the new center $\mathbf{r}_{\text{new}}$ of the grown particle is calculated through

$$\mathbf{r}_{\text{new}} = \frac{m_i\mathbf{r}_i + m_j\mathbf{r}_j}{m_i + m_j} \tag{4}$$

Due to the aforementioned complexity of the surface processes, the following considerations are taken into account: (i) the initial configuration of the substrate is perfectly flat, homogeneous and free of defects, unless stated otherwise; (ii) the initial number of metal adatoms on the surface is zero; (iii) metal adatoms are deposited randomly on the substrate or on particles that have been previously deposited; (iv) no surface desorption is allowed. This assumption is based on the fact that, by calculating the influx of adatoms from the simulated electrochemical current, surface desorption of adatoms is already taken into account in the total cathodic current since $I_{\text{Tot}} = I_{\text{Ads}} - I_{\text{Des}}$, with I_{Tot} being the net influx that results from the difference between adatom adsorption, I_{Ads}, and desorption, I_{Des}, *i.e.*, electrochemical reduction and oxidation. Further details are given elsewhere.[63] It must be noted that a similar interpretation of the reduction current in the initial stages of electrodeposition has been adopted to explain the nucleation and growth of Pd particles on carbon.[43] Furthermore, (v) the aggregation of adatoms or clusters is assumed to be irreversible; (vi) the surface diffusion coefficient of adatoms is assumed to be constant for all simulations unless otherwise stated; (vii) the shapes of the growing clusters are approximated to be spherical. Herein, it must be re-emphasized that in the present model, cluster–cluster coalescence kinetics is not considered. Therefore, when two clusters collide, coalescence is immediate. Previous experimental work in electrodeposition and soft-landed clusters shows that this approximation is valid when the deposited material has a low melting point (Ag, Cu, Sb, In) and the cluster surfaces are free of adsorbates that could hinder or delay coalescence.[36,37,82] Contrarily, the electrodeposition of materials of high melting point and/or whose surfaces are susceptible of becoming passivated by adsorbates (Pt, Pd) have shown to lead to ramified, porous and dendritic structures, due to slow or impeded coalescence.[37,43,47,82–84] In any case, although the current model does not allow predicting the morphology of the growing islands, it allows the study of magnitudes such as cluster size, cluster number density and surface coverage, since these are barely influenced by the coalescence process. Finally, (viii) no energetic considerations are taken for nucleation and the formation of clusters occurs by aggregation of particles (clusters and adatoms).

It is well known that surface defects and the Gibbs free energy of formation (which depends on the specific surface energy between the different phases, besides the overpotential) drive nucleation phenomena. This, in turn, causes the electrochemical current measured during the initial stages of potentiostatic electrodeposition to be dependent on the substrate–metal interactions. Although this is not explicitly considered in our model, it can be considered to be included in the FEM simulation of the net electrochemical current, through the kinetic constant of the silver electrochemical reduction reaction on a given substrate. This has been assumed here as the forward reaction rate, $K_{\text{f}} = 0.0001$ mol m^{-3} s^{-1} and charge transfer coefficient, $\alpha_{\text{f}} = 0.56$.[63] Besides, once clusters have reached a given size and can be considered pinned to a location on the surface (their surface diffusion coefficient becomes negligible), three-dimensional regions of reduced reactant concentration would start to develop around the growing clusters. However, this phenomenon has not been included yet in the model, since the focus of this article is on the initial stages after polarization (to the left of the red bar in the schematic current–time transient shown in Fig. 1(b)).

Different simulations have been run with different net influx factors F (*i.e.*, for different applied electrode potentials) and for relative surface mobility factors, α. The mass and radius of all metal adatoms are $m \approx 107.87$ g mol^{-1} and $R \approx 0.165$ nm, respectively. All simulations run for a physical time of 10 ms. For every considered case, five different simulations were run with different sets of random numbers and hence the mean of the properties is always presented in this paper.

3 Results and discussion

In this section, we evaluate the effect of the applied overpotential, η, and the relative surface mobility factor, α, on the cluster formation, aggregation and size distribution evolution with time. As previously explained, the effect of the overpotential is taken into account by using different influx factors ($F = 1 \sim E = -0.11$ V $\sim \eta = 560$ mV; $F = 2 \sim E = -0.18$ V $\sim \eta = 630$ mV; $F = 3 \sim E = -0.25$ V $\sim \eta = 700$ mV; $F = 4 \sim E = -0.3$ V $\sim \eta = 750$ mV). Since the mass transport conditions are the same through all the simulations, each overpotential translates directly in an influx factor, F, with a higher overpotential resulting in higher F. Besides this, different relative surface mobility factors are used ($\alpha = 0.5$, 1.0, 1.5 and 2.0), since $0.5 \leq \alpha \leq 2$ are the most common values reported in the literature.[50,51]

3.1 Evolution of the number of single adatoms

Fig. 3 shows the time evolution of the density of adatoms on the surface (n_{adatoms} [1 cm^{-2}]) as a function of time for different influx factors F, for $\alpha = 1$ (a) and different values of α for $F = 1$ (b). In all cases, the number of adatoms decreases with time. This is due to two reasons: first, the imposed influx decreases with time due to a gradual reduction of the mass transport of metal cations towards the electrode surface. Second, adatoms diffuse randomly over the electrode surface and aggregate with each other.

Increasing the net influx (*i.e.*, increasing the overpotential) results, obviously, in a higher number of adatoms at any time, as shown in Fig. 3(a). Besides this, the surface diffusion coefficient, D, also influences highly the evolution of the number of adatoms on the electrode surface. Since D_0 is constant through the simulations, the influence of the relative surface mobility factor, α, is evaluated. Fig. 3(b) shows that high values of α result in a faster depletion of adatoms in shorter times. This can be explained as follows. For higher values of α, the mobility of large clusters becomes smaller and this results in the formation of a large number of clusters of small size. Therefore, incoming adatoms have higher chances to encounter clusters to aggregate with so the number of free adatoms on the surface decreases faster.

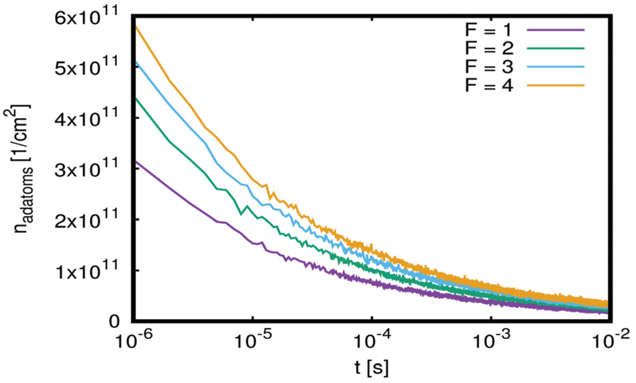

(a) α = 1.0

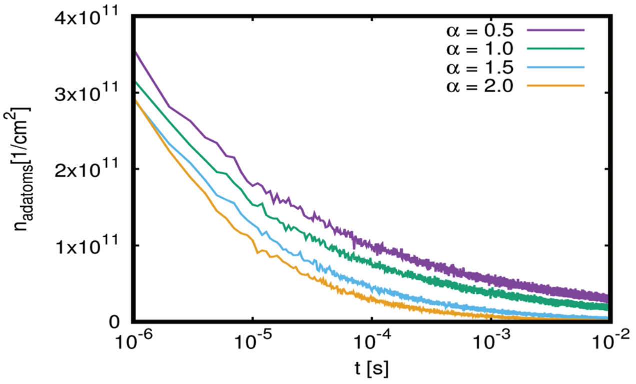

(b) F = 1

Fig. 3 Time evolution of the density of adatoms on the electrode surface for different influx factors, F, and $\alpha = 1$ (a), and for different values of α and $F = 1$ (b).

3.2 Early stages of cluster formation and aggregation

With the purpose of evaluating the influence of different parameters on the initial stages of cluster formation and growth, we define an arbitrary radius of 2 nm to define the formation of a cluster since this is approximately the size of the smallest clusters that have been imaged experimentally for Ag,[36,37] Pt[36,47] and Pd.[43] It must be noted that the analysis that follows would be similar if the arbitrary size would be different; only absolute values would change but the trends would be maintained. This is shown in Fig. S1 of the ESI,† where the evolution of the number of clusters is compared when different arbitrary radii are selected.

3.2.1 Influence of the overpotential (net flux of adatoms) on cluster formation and aggregation. Fig. 4 shows the evolution of the number N_c and density n_c [1 cm^{-2}] of metal clusters with $R \geq 2$ nm for different net influxes for $\alpha = 1$ (a) and $\alpha = 2$ (b). It can be seen that the time needed for the first cluster of $r = 2$ nm to be formed, *i.e.*, the induction time, t_{Ind}, decreases with an increase of the net flux of adatoms (*i.e.*, higher overpotential). Essentially, increasing the imposed overpotential results in a higher number of adatoms deposited on the electrode surface. Hence, this results in a faster formation of clusters by increasing the probability of adatom aggregation.

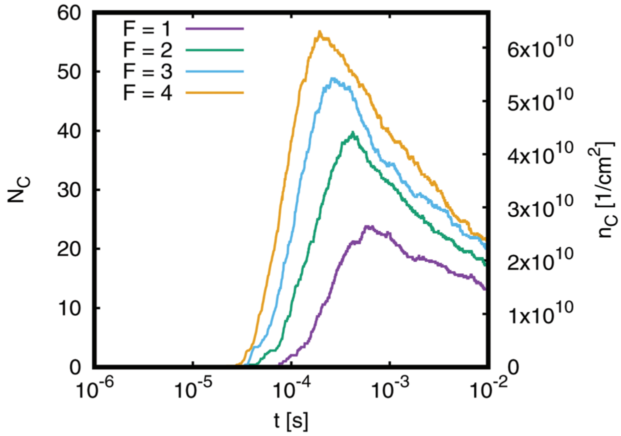

(a) α = 1.0

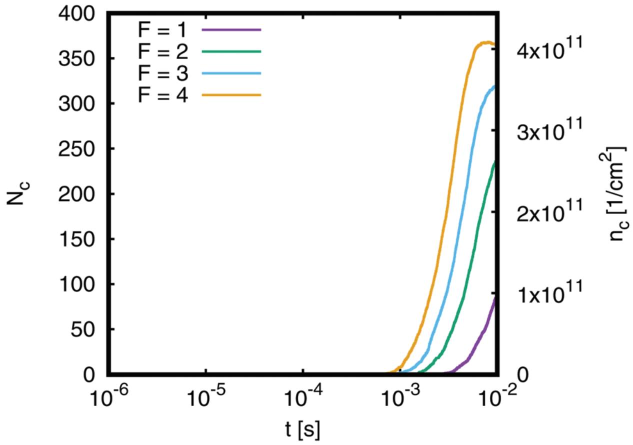

(b) α = 2.0

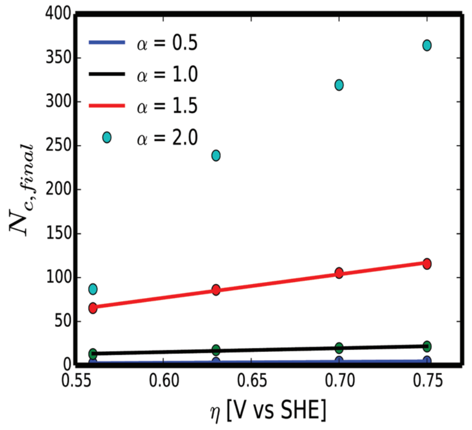

(c)

Fig. 4 The number and density of clusters larger than 2 nm on the surface as a function of time for different influxes for (a) α = 1 and (b) α = 2. (c) The number of clusters ($n_{c,\text{final}}$) after 10 ms as a function of η for different values of α. The lines show the linear fit to the simulated data.

In addition to increase the rate at which clusters are formed, this leads to shorter induction times as proved experimentally in many occasions.[18,20,41,42,66,67,85]

However, the effect of cluster mobility, represented by the relative surface mobility factor, α, is generally overlooked. For a small value of α (Fig. 4a), the number of clusters first increases, reaches a maximum and then decreases. Such a decrease, which has been previously reported experimentally,[36,37] is caused by cluster (not adatom) aggregation. This process is hereafter referred to as *nucleation–aggregation balance* and the time where $N(t)$ reaches a maximum is referred to as *nucleation–aggregation transition time* and denoted $t_{\text{Nucl–Aggr}}$. For large values of α (Fig. 4(b)), the formation of clusters is delayed (longer induction time), and a higher number of clusters are formed. Although $N(t)$ levels off for very high influxes, the number of clusters does not decrease substantially at longer times, in contrast to the case of lower α.

In the classical nucleation and growth theory, nuclei are assumed to be stable (not moving) and $N(t)$ is assumed to be represented by $N_0[1 - \exp(-At)]$ (see Introduction). These assumptions would be represented by the case in which $\alpha \to \infty$. However, it has been shown experimentally that small nanoclusters are not stable[36–38,43,47] and hence non-infinite values of α need to be considered. In fact, the $N(t)$ profiles depicted in Fig. 4(a), with α = 1, are similar to those determined experimentally for Ag electrodeposition,[37,47] indicating that the actual model of cluster surface diffusion during the initial stages of electrodeposition can be valid to interpret experimental data.

Moreover, Fig. 4(a) and (b) show that the nucleation–aggregation transition time ($t_{\text{Nucl–Aggr}}$) also depends on the imposed influx. Increasing the net flux results in a decrease of the transition time regardless of α. The reason is that, independently of the surface diffusion of the clusters, a higher flux of adatoms leads to the formation of a higher number of clusters, separated by shorter distances from each other. This implies that cluster aggregation becomes dominant at shorter time scales.

Besides, the total number of clusters with $R \geq 2$ nm after 10 ms ($N_{\text{c,final}}$) is shown in Fig. 4(c). One can see that $N_{\text{c,final}}$ increases linearly with the overpotential, regardless of the relative diffusion factor (α), for small values of α. When $\alpha \geq 2$, the number of clusters after a given time also increases with overpotential but seems to level-off for large η. The effect of α on $N(t)$ is further discussed in section 3.2.3.

3.2.2 Influence of the overpotential (net flux of adatoms) on the size of clusters.

Fig. 5 displays the size evolution of the largest cluster as a function of time for different net fluxes for α = 1 (a) and α = 2 (b). Regardless of the relative surface mobility factor α, the radius of the largest cluster follows a square root time dependence $(R_{\max} \propto \sqrt{t})$, typical of diffusion controlled growth. The size of the largest cluster ($R_{\max,\text{final}}$) after 10 ms as a function of overpotential, for different values of α, is displayed in Fig. 5(c). The size of the largest cluster increases linearly with the overpotential, regardless of α. This is logical, since increasing the overpotential results in a higher flux of adatoms, faster cluster formation and a slight increase in cluster size.[68,85,86] The effect of α on the size of the clusters is further discussed in section 3.2.3.

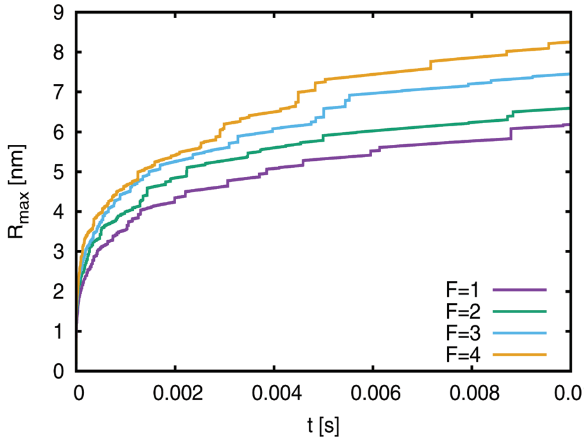

(a) α = 1.0

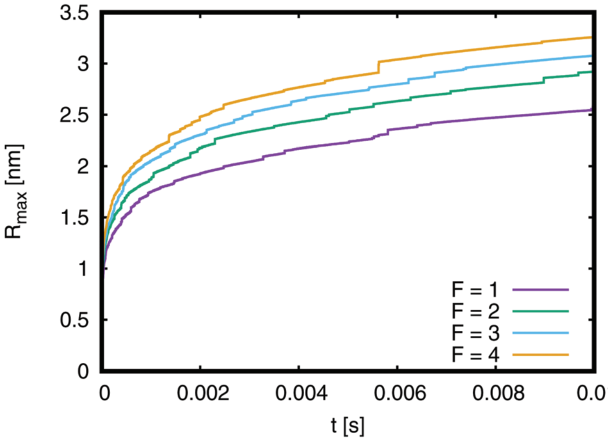

(b) α = 2.0

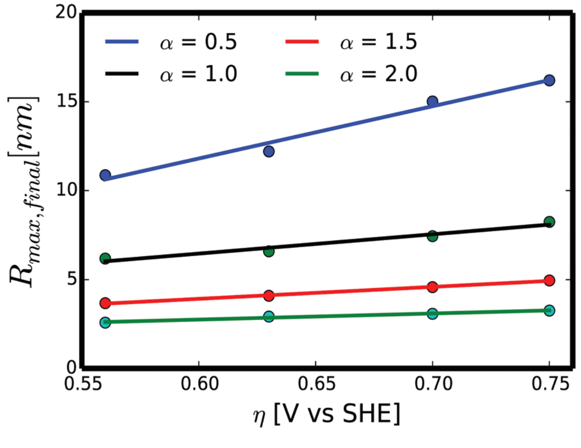

(c)

Fig. 5 The size of the largest cluster, $R_{\max}$, as a function of time for different influxes for α = 1.0 (a) and α = 2.0 (b). (c) The size of the largest cluster after 10 ms, $R_{\max,\text{final}}$, as a function of η for different values of α. The lines show the linear fit to the simulated data.

3.2.3 Influence of the relative surface mobility factor α on cluster formation and aggregation. Although increasing the net flux (*i.e.*, overpotential) always results in a higher cluster formation rate and faster growth, it is already evident from Fig. 3 and 4 that the relative surface mobility factor, α, generally overlooked in electrochemical nucleation and growth phenomena, also plays an important role.

Fig. 6(a) and (b) show the evolution of the number and density of clusters with time for different relative surface mobility factors for F = 1 (a) and F = 4 (b). $N(t)$ shows a similar trend in all considered cases. After a certain induction time, t_{Ind}, the number of clusters first increases (cluster formation), reaches a maximum at $t_{\text{Nucl–Aggr}}$ (nucleation–aggregation balance) and then decreases due to the prevalence of cluster aggregation to the formation of new clusters. Cluster aggregation processes are especially relevant in electrochemical deposition under stagnant conditions since the influx of adatoms decreases very fast after the application of a given overpotential due to the diffusion driven transport of species from the bulk solution to the electrochemical interface. This implies that the probability of formation of new nuclei decreases substantially with time. Therefore, it is not surprising that cluster aggregation results in a decrease of the number of clusters on the surface, this decrease not being overcome by the formation of new clusters.

In all considered cases, regardless of the net flux, increasing α leads to longer induction times, indicating that the formation of clusters requires longer time. Herein, it must be noted that an arbitrary radius of 2 nm has been considered to define a cluster. However, although the absolute values of t_{Ind}, N_{C} and $t_{\text{Nucl–Aggr}}$ are affected by the arbitrary size defined to differentiate between adatom aggregates and clusters, the analysis is valid independent of the selected arbitrary size (see ESI, Fig. S1†). The fact that a higher α delays the formation of clusters is logical, since a larger α means that adatom-aggregates formed by more than 1 atom diffuse slower on the surface. Hence, since clusters are formed not only by the incorporation of adatoms but also by the incorporation of adatom aggregates, a slower diffusion of the latest induces a longer induction time.

Furthermore, it can be noticed in the same figures that an increase in α results in a positive shift of the nucleation–aggregation transition time, $t_{\text{Nucl–Aggr}}$, *i.e.*, the peak of n_{c} *vs.* t. This indicates that cluster aggregation becomes prevalent only at longer times. This is also logical since an increase in α results in decreasing of cluster mobility and therefore prevents existing clusters to aggregate for longer times.

The effect of the relative surface mobility factor on the final number of clusters after 10 ms of deposition for different influxes F is shown in Fig. 6(c). It shows that increasing α yields an increase of the final number of clusters. This implies that for small mobility, *i.e.* larger α, cluster formation is favoured compared to cluster aggregation, which results in a higher particle density. Interestingly, Fig. 6(c) also indicates that the number of clusters at any time during the early stages of electrochemical deposition is more dependent on cluster mobility than on the overpotential itself.

3.2.4 Definition of $N(t)$ in electrochemical deposition. After the application of a step potential, the evolution of the number of clusters with time is usually understood as the number of nuclei which are formed at the substrate and is given by[19,20,85]

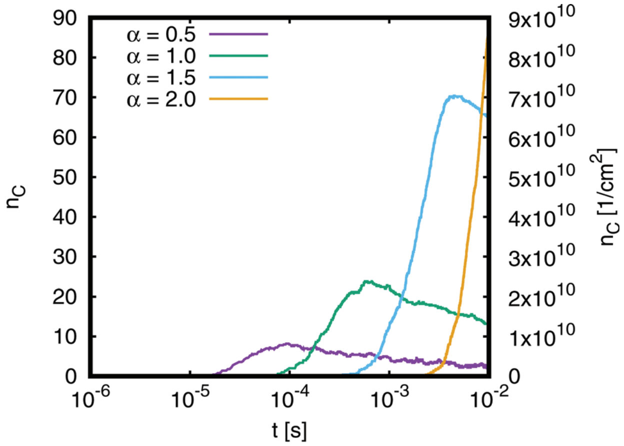

(a) F = 1

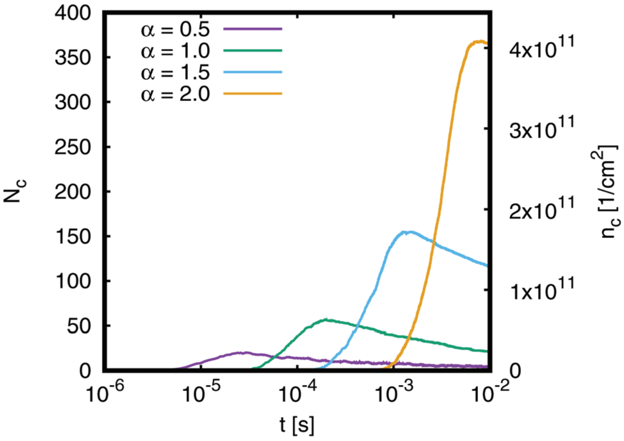

(b) F = 4

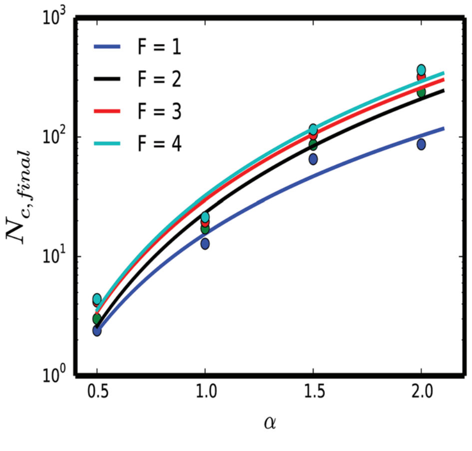

(c)

Fig. 6 The number and density of clusters larger than 2 nm on the surface as a function of time for different values of α at (a) F = 1 and (b) F = 4. (c) The final number of clusters ($n_{c,\text{final}}$) after 10 ms as a function of α at F = 1.

$$N(t) = N_0[1 - \exp(-A_0 \times t)] \tag{5}$$

where N_0 is the nucleation saturation number density and A_0 is the nucleation rate constant. Such equation can also be corrected to account for an induction time,[32,40,42,87,88] which accounts for the stochastic processes occurring prior to the formation of stable nuclei:

$$N(t) = N_0[1 - \exp(-A_0 \times (t - t_{\text{IND}}))] \tag{6}$$

However, such a definition for $N(t)$ considers that once a stable nucleus is formed, it is fixed at the substrate. Hence, $N(t)$ increases monotonically. A large variety of previous experimental studies have shown that the evolution of clusters with time can indeed be represented by eqn (5) or (6).[32,87–90] However, it was recently demonstrated that, although this was the case when clusters of $d \geq 5$ nm were probed, the analysis of the surfaces with high resolution TEM yielded a population of small clusters of $d \approx 1$–2 nm that followed $N(t)$ profiles such as those shown in Fig. 6.

This can be attributed to nanocluster mobility and aggregation when non-infinite values of α are considered. Fig. 7 shows the $N(t)$ profiles considering clusters larger than several arbitrary sizes for $\alpha = 1$. It shows that, even if aggregation of small nanoclusters occurs, $N(t)$ could still be represented by eqn (6), when only clusters of $R \geq 5$ nm are probed (equivalent to image the surface with FESEM instead of TEM).[36]

This demonstrates that the nucleation rate cannot be determined by counting clusters on the electrode surface unless it is guaranteed that the entire cluster population, including $d \approx$ 1–5 nm, is probed. Even in that scenario, unless the number of clusters is captured at very short times after the application of a given overpotential, $N(t)$ would not represent the number of nuclei, but the number of aggregated clusters.

The total number of clusters considering aggregation, $N_{\text{CLUSTERS}}(t)$, could then be related to the real number of nuclei, $N_{\text{NUCLEI}}(t)$, by taking into account aggregation kinetics. $N_{\text{NUCLEI}}(t)$ would be described by

$$N_{\text{NUCLEI}}(t) = N_{\text{INF}} \times (1 - \exp[-A_{\text{NUCL}} \times (t - t_{\text{IND}})]) \tag{7}$$

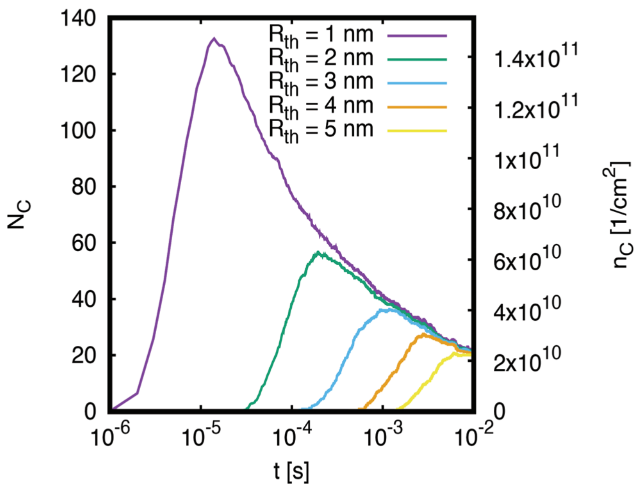

Fig. 7 The number and density of clusters, larger than a given size (R = 1 nm, 2 nm, 3 nm, 4 nm and 5 nm) as a function of time for α = 1 and F = 4.

where N_{INF} is the nucleation saturation number density and A_{NUCL} is the real nucleation rate constant. The number of clusters on the surface, $N_{\mathrm{CLUSTERS}}(t)$, could then be expressed by

$$N_{\mathrm{CLUSTERS}}(t) = N_{\mathrm{NUCLEI}}(t) \times B \times (1 + \exp[-A_{\mathrm{AGG}} \times (t - t_{\mathrm{IND}})] \tag{8}$$

where A_{AGG} is the aggregation rate constant which is dependent on the overpotential, and also dependent on α and D_0 since it relates to the surface mobility of the clusters; at longer time $N_{\mathrm{NUCLEI}}(t) \times B$ is equivalent to N_0 of eqn (6) where $0 < B \leq 0.5$, which is the saturation of bigger cluster number density. From the data shown in Fig. 6, it can also be deduced that t_{IND} has an exponential dependence on α ($t_{\mathrm{IND}} = K_1 \times \exp(K_2 \times \alpha)$).

It is not the aim of this article to discuss the nucleation process itself, since no energetic considerations have been evaluated for nucleation (see section 3.2) and the critical size for nucleation has not been assumed. However, we show that, independently of the nucleation process that drives $N_{\mathrm{NUCLEI}}(t)$, the cluster surface mobility plays a major role in the number of clusters that eventually grow stable on the surface, $N_{\mathrm{CLUSTERS}}(t)$. Fig. 8(a) shows schematically $N_{\mathrm{NUCLEI}}(t)$ (black) and $N_{\mathrm{CLUSTERS}}(t)$ (red) using eqn (7) and (8), respectively. For comparison, $N_{\mathrm{CLASSIC}}(t)$ (blue) shows the $N(t)$ profile that would be incorrectly determined if very small clusters are not resolved or only long deposition times are considered. Herein it must be borne in mind that 'long' deposition times can be as short as milliseconds,[36] depending on the experimental conditions.

Fig. 8(b) shows the effect of the parameter that describes aggregation kinetics on the resulting $N_{\mathrm{CLUSTERS}}(t)$ for a fixed $N_{\mathrm{NUCLEI}}(t)$. When the rate of aggregation is very slow ($A_{\mathrm{AGG}} \to 0$, which implies $D_0 \to 0$ or $\alpha \to \infty$ respectively), the deviation between $N_{\mathrm{CLUSTERS}}(t)$ (eqn (8)) and $N_{\mathrm{NUCLEI}}(t)$ (eqn (7)) becomes insignificant and both curves overlap. This means that, in the case that cluster mobility is slow compared to the birth of new nuclei, the number of growing clusters, $N_{\mathrm{CLUSTERS}}(t)$, and the number of formed nuclei, $N_{\mathrm{NUCL}}(t)$, would be equivalent. However, when the rate of aggregation is non-negligible, the number of growing clusters would be significantly lower than the number of nuclei.

The models available to fit *I*–*t* transients[19–28] are based on considering $N(t)$ (eqn (5)) as the number of clusters which grow by direct attachment. This implies that, by fitting *I*–*t* transients, A_0 and N_0 do not correspond to real nucleation kinetic parameters, but rather to the kinetics of formation of stable, large enough clusters that are fixed on the substrate and grow by direct attachment. Therefore, if cluster aggregation is overlooked, this procedure will always result in an underestimation of nucleation kinetic parameters by several orders of magnitude.[36,37,91] As a consequence, this could explain the large scatter, up to 5 orders of magnitude, of nucleation rates and saturation number densities reported experimentally by either fitting chronoamperometric data or by imaging (*in situ* or *ex situ*) the evolution of the number of aggregated clusters with time.[89]

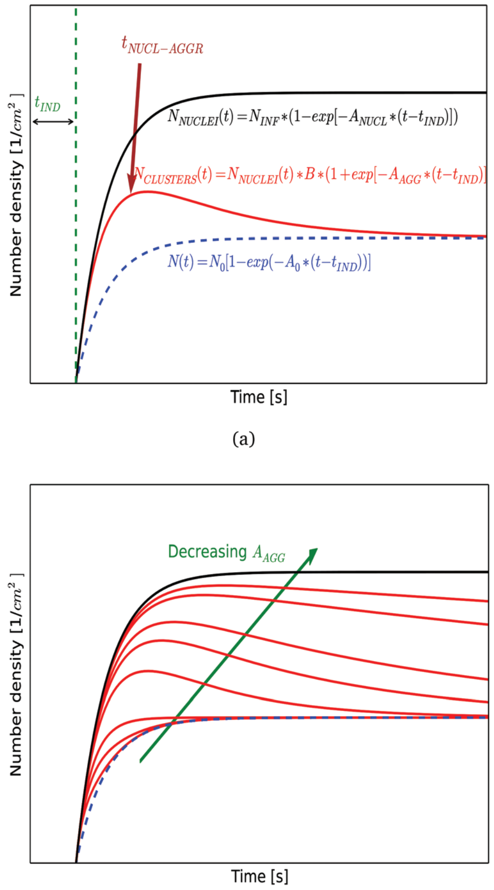

(a)

(b)

Fig. 8 (a) Schematic representation of different $N(t)$: (black) the total number of nuclei, (red) the number of clusters taking aggregation into account and (blue) the incorrect number of nuclei that would be determined when aggregation is not considered. (b) The effect of A_{AGG} on $N_{\mathrm{CLUSTERS}}(t)$ for a fixed nucleation rate.

Moreover, it also becomes clear from Fig. 6 and 8 that the progressive ($A_{\mathrm{NUCL}} \to 0$) or instantaneous ($A_{\mathrm{NUCL}} \to \infty$) character of the nucleation process cannot be easily determined from an experimental evaluation of $N(t)$ since the number of growing clusters, *i.e.*, the ones that can be experimentally probed, do not reflect only nucleation, but also aggregation kinetics.

3.2.5 Influence of the relative surface mobility on the cluster size distributions. Fig. 9(a) shows the radius of the largest cluster ($R_{\max}$) as a function of time for different values of α at $F = 1$. It can be seen that the size of the largest cluster decreases significantly with increasing α, regardless of the imposed influx. This confirms again the information inferred previously from Fig. 5 and 6. Since a large value of α results in slow cluster diffusion on the electrode surface, cluster growth under these conditions is mainly due to the incorporation of adatoms rather than cluster aggregation or incorporation of large adatom aggregates.

Fig. 9(b) shows the size of the largest cluster ($R_{\max,\mathrm{final}}$) after 10 ms of deposition, as a function of α. The plot clearly shows that increasing the value of α results in a decrease of the size

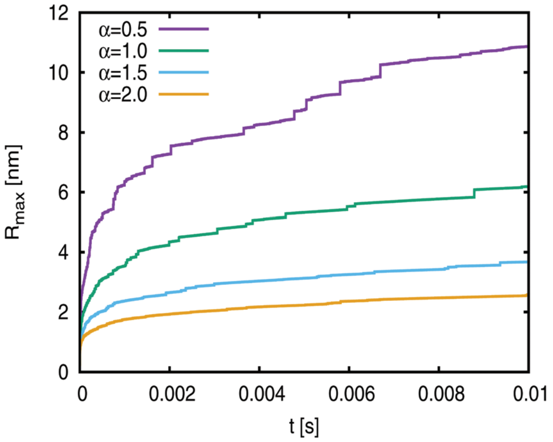

(a) F = 1

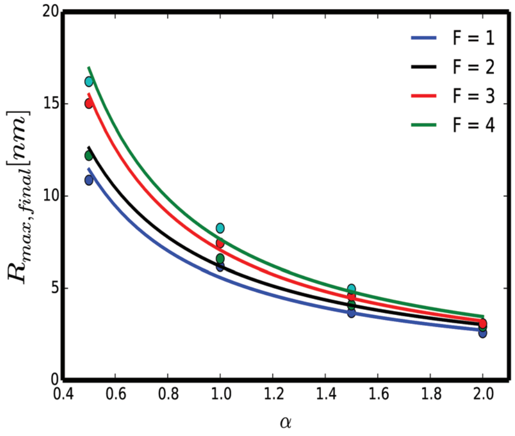

(b)

Fig. 9 The size of the largest cluster, R_{max}, as a function of time for different values of α at F = 1 (a). The size of the largest cluster after 10 ms, $R_{\text{max,final}}$, as a function of α for F = 1 (c); the lines show the trend.

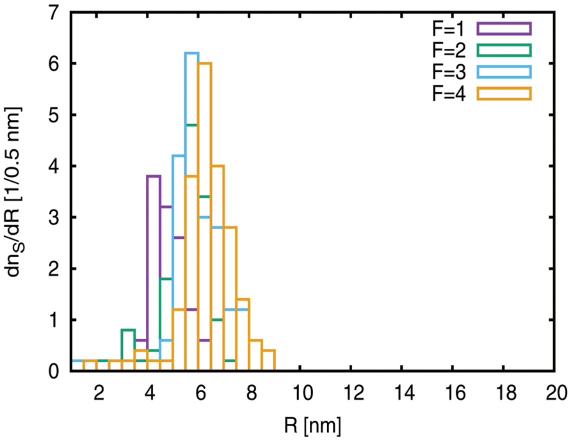

(a) α = 1.0

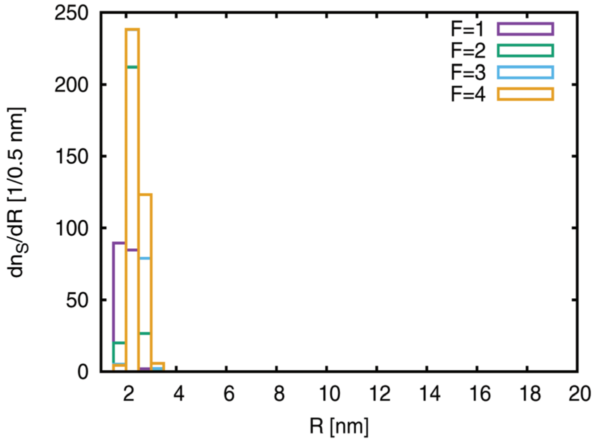

(b) α = 2.0

Fig. 10 The particle size distribution for different influxes for α = 1 (a) and α = 2 (b) after 10 ms deposition.

of the largest cluster by following a power law. Interestingly, it indicates that the cluster size is more dependent on cluster mobility than on the overpotential itself.

The histograms of the size distribution of all the individual particles on the electrode surface as a function of time are shown in ESI, Fig. S2.† Increasing the deposition time results in a larger dispersion of the particle sizes and in a decrease of the number of adatoms and small adatom aggregates. The effect of the net flux on the particle size distribution for α = 1 and α = 2 after 10 ms is shown in Fig. 10(a) and (b), respectively. The histogram shows that increasing or decreasing the net flux (overpotential) has an important effect on the number of particles on the surface but a slight influence on the particle size distribution. However, by comparing the distribution for α = 1 (Fig. 10(a)) with that for α = 2 (Fig. 10(b)), it can be clearly seen that a change in α affects the particle size distribution much more significantly. The higher the relative surface mobility factor is (*i.e.*, lower mobility of large clusters), the narrower the particle size dispersion is. This re-emphasizes the need for controlling not only the overpotential, but also the surface diffusion of adatoms and clusters to tune the electrodeposited cluster size distribution precisely.

3.3 Mutual influence of influx and mobility

In summary, the competition between adatom deposition and aggregation processes implies that the magnitudes that describe a distribution of supported nanoclusters during the early stages of electrochemical deposition (cluster radius, R; cluster size dispersion, σ_R; cluster number density, N; and surface coverage, SC) can be rationalized with respect to the overpotential (η) and the relative surface mobility factor (α). This is schematically shown in Fig. 11. Increasing η results in denser distributions of larger clusters with larger size dispersion. More importantly, the effect of α is much more pronounced. For any η, a large α (low nanocluster mobility) implies obtaining much denser distributions of smaller clusters with a narrower size distribution.

The consideration of nanocluster aggregative processes in the early stages of electrochemical deposition is still quite

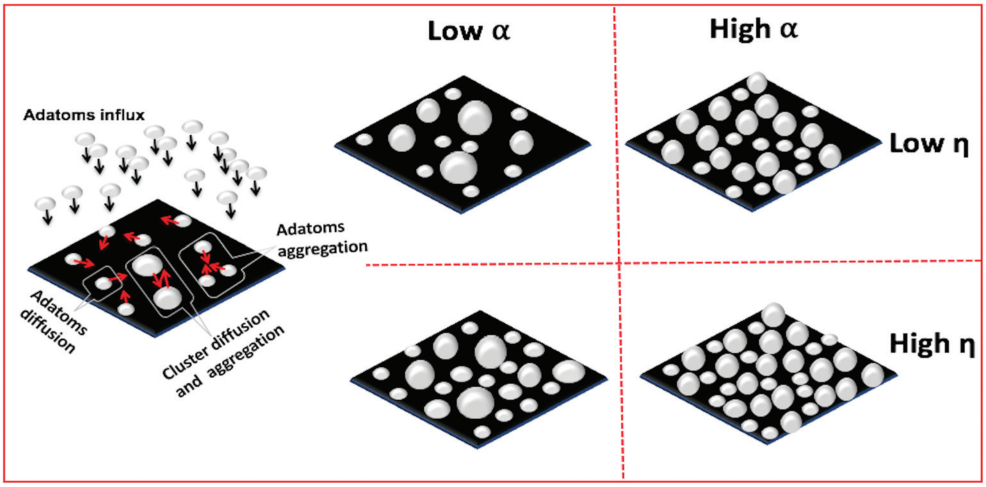

Fig. 11 (Left) Schematic representation of the simulated fundamental processes during the early stages of electrochemical growth: deposition and aggregation. (Right) Schematic representation of the effect of overpotential (η) and relative surface mobility factor (α) on the magnitudes that describe the distribution of supported nanoclusters: size distribution, number density and surface coverage.

recent and, thus, the amount of dedicated experiments to study these processes is still scarce. However, the trends shown schematically in Fig. 11 can be qualitatively compared to distinct electrochemical deposition systems. Ag (high D_0, low α) and Pt (low D_0, high α) electrodeposition on glassy carbon from aqueous solutions with high overpotentials are taken for comparison.[37] Ag electrodeposition results in lower N, lower SC, larger R and larger σ_R compared to Pt electrodeposition. Although the electrochemical deposition kinetics of Ag is much faster than that of Pt (higher adatom flux for the same applied overpotential), the differences in the cluster distributions have been shown to be also related to the differences in the surface mobility and coalescence kinetics of small nanoclusters, the latter not considered in this article. Similarly, a higher density of smaller nanoclusters is generally obtained after the electrodeposition of different metals from highly viscous and less conductive deep eutectic solvents.[91,92] This is also likely to be related to hindered aggregation and coalescence processes and not only to slower electrochemical kinetics.

3.4 Influence of surface defects on cluster formation and aggregation

All throughout the discussion above, a homogeneous, flat and defect free surface has been assumed. However, this is never the case in a real electrodeposition experiment. Therefore, simulations were also performed by taking into account defects on the electrode surface which trap all clusters of $R \geq 2$ nm, so they are no longer mobile, *i.e.*, $D(R \geq 2\text{ nm}) = 0$.

Fig. 12 compares the evolution of the density of adatoms n_{adatoms} and clusters n_c (a) and of the size of the largest cluster (b) on a defect-free surface (WOD) and on a surface with defects (WD), as a function of time for F = 1 and α =

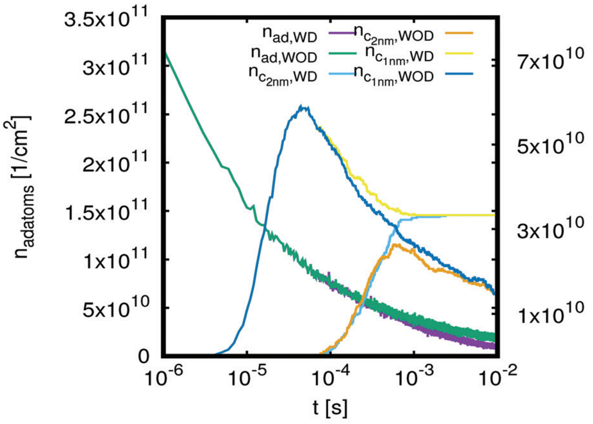

(a) F = α = 1.0

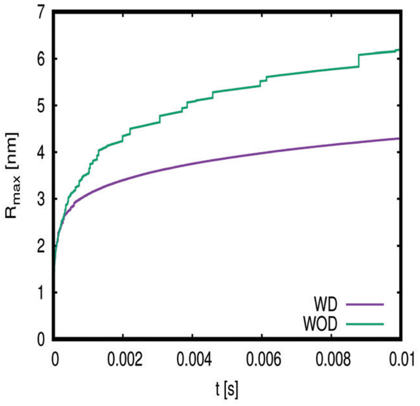

(b) F = α = 1.0

Fig. 12 (a) Evolution with time of the density of adatoms and clusters of $R \geq 1$ nm and $R \geq 2$ nm on a surface with (WD) and without (WOD) defects. (b) Size evolution of the largest cluster on a surface with (WD) and without (WOD) defects. In both cases, F = 1 and α = 1.

1. Fig. 12(a) indicates that, although the evolution of the density of adatoms with time coincides, the same does not hold for the evolution of the density of clusters. Within a short time range, before the cluster formation–aggregation balance, the two curves coincide. However, at longer times, the two curves differ substantially, since the growth mechanisms are highly different. In the case of a defect-free surface, WOD, the cluster density decreases with time, as shown in section 2, due to an aggregative growth process, since clusters of $R \geq 2$ nm are still mobile. Contrarily, in the case of a surface with a given concentration of surface defects (WD) which trap all clusters of $R \geq 2$ nm, the number of clusters eventually saturates. It is again interesting to compare what happens if only clusters larger than a given size are considered. If only clusters with $R \geq 2$ nm are considered, no apparent aggregation occurs, *i.e.*, $N(t)$ increases monotonically until it saturates, since all these clusters are trapped by defects on the surface. However, if all the clusters with $R \geq 1$ nm are considered, $N(t)$ first increases, then decreases due to aggregation and only then saturates. This proves again that if small clusters are missed due to limitations in the resolution of the surface characterization technique, or if the evaluation of the number of clusters is carried out only when it reaches saturation, no conclusion on the nucleation can be extracted since the evaluation of $(N(t))$ reflects both nucleation and aggregation kinetics.

In addition, Fig. 12(b) shows the evolution of the largest cluster as a function of time for both (WD and WOD) cases. It becomes clear that in the case that the surface is highly defective, the size of the largest cluster increases very slowly, whereas in the case of a defect-free surface, it grows comparatively fast due to the incorporation/aggregation of mobile clusters. In general, Fig. 12 indicates that in a highly defective surface, the trapping of mobile nanoclusters slows down cluster growth and enhances cluster formation which results in larger cluster densities.[34] This would explain the large cluster densities obtained when electrodeposition is carried out from highly viscous non-aqueous electrolytes[92] since a high number density can be attributed to impeded nanocluster mobility and not only to differences in the electrochemical reduction kinetics.

3.5 Influence of the surface mobility of adatoms (D_0)

In the previous sections, the effect of the relative surface mobility factor, α, on the nanocluster growth mechanisms has been discussed, where α depends on how different is the binding energy between adatoms of a given material and between them and the substrate.[50–52] However, the mobility of adatoms on the substrate itself, determined by D_0, also plays a role in determining how cluster growth proceeds in the initial stages of electrodeposition. In this context, it has been shown that varying the surface diffusion of adatoms can induce the formation of different nanostructures[59] and could influence the number, size and surface coverage. In order to evaluate the influence of the adatom surface diffusion coefficient, D_0, we performed simulations with different values of D_0 ($D_0 = 2 \times 10^{-9}$ m^2 s^{-1} and 8×10^{-9} m^2 s^{-1}) and different values of α (α = 0.5 and 1.0). The evolution of the number and density of clusters as a function of time for two different values of D_0 and α at $F = 1$ is shown in Fig. 13(a).

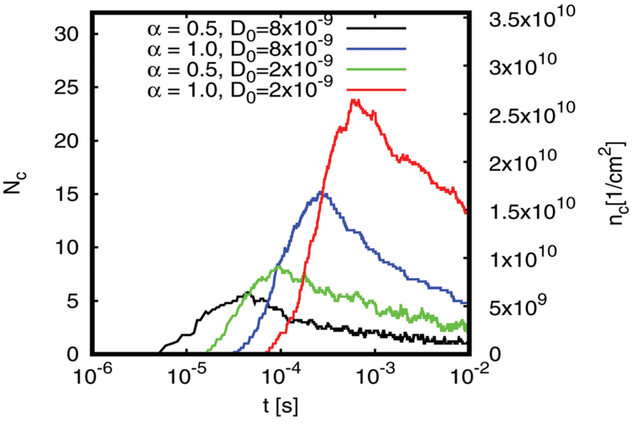

(a) F = 1

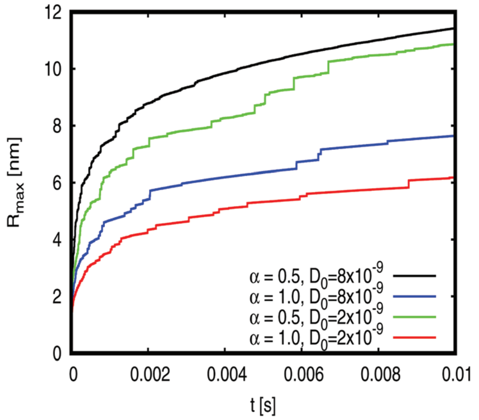

(b) F = 1

Fig. 13 The evolution with time of the number and density of clusters (a) and of the size evolution of the largest cluster (b) as a function of time for different adatom surface diffusion coefficients (D_0) and relative surface mobility factors (α) for $F = 1$.

Increasing D_0 results in a slight decrease of the number of clusters, and a shift to shorter times of both the induction time and the cluster formation–aggregation balance. This is reasonable because a higher mobility of the adatoms leads to a quicker formation of clusters. Since the mobility of larger clusters is also proportional to D_0, cluster aggregation also proceeds faster. Besides this, D_0 also influences the size of the largest cluster, as shown in Fig. 13(b). Increasing D_0 leads to a slight increase in the cluster size due to a quicker assimilation of adatoms into the existing clusters.

However, the influence of relative surface mobility factor (α) on both the cluster number and size is more significant than that of D_0. This indicates that deviations between experimental data and analytical and/or numerical models are not only due to the under/overestimation of the mobility of adatoms. Instead, the extent to which clusters of few nm in diameter are able to move on the surface, mathematically represented by α, plays a more crucial role, as anticipated experimentally.[36–38,43] Therefore, to properly understand the early stages of electrodeposition, it is necessary to take into account an electrochemical aggregative growth mechanism that considers the contributions of the mobility of both adatoms and clusters of up to few nm in diameter.

4. Conclusions and outlook

A novel modelling approach that couples a finite element method with a random walk algorithm has been developed to study the early stages of electrochemical cluster formation and growth at the nanoscale. Such a modelling approach provides crucial insights into the influence of different factors in the electrochemical growth process. Not only the overpotential, the transport of active species and the electrochemical kinetics are evaluated, but also the surface diffusion and aggregation of adatoms and small nanoclusters, generally overlooked in electrochemical nucleation and growth models, are taken into account.

The simulation results reveal that the nanocluster surface mobility plays a crucial role in the early growth stages, influencing the evolution of the number of clusters and their size distribution, more dramatically than the applied overpotential itself. As a result, it is shown that nucleation kinetics alone is not able to describe the evolution of the number of clusters with time ($N(t)$) in potentiostatic electrodeposition. Instead, a more accurate representation of the evolution of the number of clusters is provided, in which the balance between cluster formation (*i.e.*, nucleation) and aggregation is also considered. As such, two regimes are defined, in which either nucleation or aggregation is predominant. We show that an evaluation of $N(t)$, which neglects the effect of nanocluster mobility and aggregation, can induce errors of several orders of magnitude in the determination of nucleation rate constants.

These findings are extremely important towards evaluating the elementary process of electrodeposition, considering not only adatoms, but also nanoclusters as building blocks. The possibilities of using a coupled FEM–random walk algorithm that considers surface diffusion of both adatoms and clusters, continuous deposition, aggregation and growth are interesting in a wide range of scientific disciplines. In this context, work is already underway in systematically investigating the effects of cluster desorption, competitive chemical and electrochemical reactions as well as heterogeneous surfaces and, more importantly, energetic considerations for the nucleation process.

Conflicts of interest

There are no conflicts to declare.

Acknowledgements

Mesfin Haile Mamme acknowledges funding from the Fonds Wetenschappelijk Onderzoek in Flanders (FWO, project G019014N). Jon Ustarroz acknowledges funding from the Fonds Wetenschappelijk Onderzoek in Flanders (FWO, postdoctoral grant 12I7816N). Christoph Köhn acknowledges funding from the People Programme (Marie Curie Actions) of the European Union – Seventh Framework Programme (FP7/2007–2013) under REA grant agreement no 609405 (COFUNDPostdocDTU).

References

1 P. Milan and S. Mordechay, *Fundamental of Electrochemical Deposition*, John Wiley & Sons, 2nd edn, 2006, pp. 1–374.
2 A. Brenner and G. E. Riddell, *Plat. Surf. Finish.*, 1946, **37**, 31–34.
3 G. Staikov, in *Electrocrystallization in Nanotechnology*, ed. S. Georgi, Wiley-VCH Verlag GmbH & Co. KGaA, Weinheim, Germany, 2007, ch. 1, pp. I–XIV.
4 X. Luo, A. Morrin, A. Killard and M. Smyth, *Electroanalysis*, 2006, **18**, 319–326.
5 C. Welch, A. Simm and R. Compton, *Electroanalysis*, 2006, **18**, 965–970.
6 F. W. Campbell and R. G. Compton, *Anal. Bioanal. Chem.*, 2010, **396**, 241–259.
7 L. Rassaei, F. Marken, M. Sillanpää, M. Amiri, C. M. Cirtiu and M. Sillanpää, *TrAC, Trends Anal. Chem.*, 2011, **30**, 1704–1715.
8 J. Campelo, D. Luna, R. Luque, J. Marinas and A. Romero, *ChemSusChem*, 2009, **2**, 18–45.
9 A. Chen and P. Holt-Hindle, *Chem. Rev.*, 2010, **110**, 3767–3804.
10 A. Mohanty, N. Garg and R. Jin, *Angew. Chem., Int. Ed.*, 2010, **49**, 4962–4966.
11 W. Yu, M. D. Porosoff and J. G. Chen, *Chem. Rev.*, 2012, **112**, 5780–5817.
12 E. Budevski, G. Staikov and W. Lorenz, *Electrochemical phase formation and growth: an introduction to the initial stages of metal deposition*, VCH, 1996, p. 410.
13 F. Pena-Pereira, R. M. Duarte and A. C. Duarte, *TrAC, Trends Anal. Chem.*, 2012, **40**, 90–105.
14 T. Brülle, W. Ju, P. Niedermayr, A. Denisenko, O. Paschos, O. Schneider and U. Stimming, *Molecules*, 2011, **16**, 10059–10077.
15 A. Milchev, *Russ. J. Electrochem.*, 2008, **44**, 619–645.
16 M. E. Hyde and R. G. Compton, *J. Electroanal. Chem.*, 2003, **549**, 1–12.
17 E. Budevski, G. Staikov and W. Lorenz, *Electrochim. Acta*, 2000, **45**, 2559–2574.
18 A. Radisic, P. M. Vereecken, J. B. Hannon, P. C. Searson and F. M. Ross, *Nano Lett.*, 2006, **6**, 238–242.
19 B. Scharifker and G. Hills, *Electrochim. Acta*, 1983, **28**, 879–889.

20 B. Scharifker and J. Mostany, *J. Electroanal. Chem. Interfacial Electrochem.*, 1984, **177**, 13–23.

21 M. Mirkin and A. Nilov, *J. Electroanal. Chem. Interfacial Electrochem.*, 1990, **283**, 35–51.

22 L. Heerman and A. Tarallo, *J. Electroanal. Chem.*, 1999, **470**, 70–76.

23 A. Milchev, *J. Electroanal. Chem.*, 1998, **457**, 35–46.

24 A. Milchev, *J. Electroanal. Chem.*, 1998, **457**, 47–52.

25 M. Sluyters-Rehbach, J. Wijenberg, E. Bosco and J. Sluyters, *J. Electroanal. Chem. Interfacial Electrochem.*, 1987, **236**, 1–20.

26 M. Palomar-Pardavé, B. Scharifker, E. Arce and M. Romero-Romo, *Electrochim. Acta*, 2005, **50**, 4736–4745.

27 M. Rezaei, S. H. Tabaian and D. F. Haghshenas, *Electrochim. Acta*, 2013, **87**, 381–387.

28 A. Milchev and T. Zapryanova, *Electrochim. Acta*, 2006, **51**, 4916–4921.

29 P. Altimari and F. Pagnanelli, *Electrochim. Acta*, 2016, **206**, 116–126.

30 A. Serruya, B. Scharifker, I. Gonzï£ilez, M. Oropeza and M. Palomar-Pardavï£i, *J. Appl. Electrochem.*, 1996, **26**, 451–457.

31 R. M. Stiger, S. Gorer, B. Craft and R. M. Penner, *Langmuir*, 1999, **15**, 790–798.

32 D. Gonnissen, W. Simons and A. Hubin, *J. Electroanal. Chem.*, 1997, **435**, 149–155.

33 J. V. Zoval, R. M. Stiger, P. R. Biernacki and R. M. Penner, *J. Phys. Chem.*, 1996, **100**, 837–844.

34 F. Gloaguen, J. Léger, C. Lamy, A. Marmann, U. Stimming and R. Vogel, *Electrochim. Acta*, 1999, **44**, 1805–1816.

35 J. W. Jacobs, *J. Electroanal. Chem. Interfacial Electrochem.*, 1988, **247**, 135–144.

36 J. Ustarroz, X. Ke, A. Hubin, S. Bals and H. Terryn, *J. Phys. Chem. C*, 2012, **116**, 2322–2329.

37 J. Ustarroz, J. A. Hammons, T. Altantzis, A. Hubin, S. Bals and H. Terryn, *J. Am. Chem. Soc.*, 2013, **135**, 11550–11561.

38 S. C. S. Lai, R. A. Lazenby, P. M. Kirkman and P. R. Unwin, *Chem. Sci.*, 2014, **6**, 1126–1138.

39 J. Ustarroz, U. Gupta, A. Hubin, S. Bals and H. Terryn, *Electrochem. Commun.*, 2010, **12**, 1706–1709.

40 R. L. Harniman, D. Plana, G. H. Carter, K. A. Bradley, M. J. Miles and D. J. Fermín, *Nat. Commun.*, 2017, **8**, 971.

41 J. Velmurugan, J.-M. Noël, W. Nogala and M. V. Mirkin, *Chem. Sci.*, 2012, **3**, 3307.

42 J. Velmurugan, J.-M. Noël and M. V. Mirkin, *Chem. Sci.*, 2014, **5**, 189.

43 Y.-R. Kim, S. C. S. Lai, K. McKelvey, G. Zhang, D. Perry, T. S. Miller and P. R. Unwin, *J. Phys. Chem. C*, 2015, **119**, 17389–17397.

44 A. N. Simonov, O. V. Cherstiouk, S. Y. Vassiliev, V. I. Zaikovskii, A. Y. Filatov, N. A. Rudina, E. R. Savinova and G. A. Tsirlina, *Electrochim. Acta*, 2014, **150**, 279–289.

45 R. Wang, U. Bertocci, H. Tan, L. A. Bendersky and T. P. Moffat, *J. Phys. Chem. C*, 2016, **120**, 16228–16237.

46 Y. Liu, D. Gokcen, U. Bertocci and T. P. Moffat, *Science*, 2012, **338**, 1327–1330.

47 J. Ustarroz, T. Altantzis, J. A. Hammons, A. Hubin, S. Bals and H. Terryn, *Chem. Mater.*, 2014, **26**, 2396–2406.

48 N. Hodnik, G. Dehm and K. J. Mayrhofer, *Acc. Chem. Res.*, 2016, **49**, 2015–2022.

49 Y. Kajikawa and S. Noda, *Appl. Surf. Sci.*, 2005, **245**, 281–289.

50 P. Jensen, A.-L. Barabási, H. Larralde, S. Havlin and H. E. Stanley, *Phys. Rev. E: Stat. Phys., Plasmas, Fluids, Relat. Interdiscip. Top.*, 1994, **50**, 618–621.

51 P. Jensen, *Rev. Mod. Phys.*, 1999, **71**, 1695–1735.

52 P. Jensen, A.-L. Barabási, H. Larralde, S. Havlin and H. Stanley, *Chaos, Solitons Fractals*, 1995, **6**, 227–236.

53 *Fractals and Disordered Systems*, ed. A. Bunde and S. Havlin, Springer Berlin Heidelberg, Berlin, Heidelberg, 1991.

54 T. Vicsek, *Phys. Rev. Lett.*, 1984, **53**, 2281–2284.

55 Y. Cao and A. C. West, *J. Electroanal. Chem.*, 2001, **514**, 103–108.

56 Y. Cao, P. C. Searson and A. C. West, *J. Electrochem. Soc.*, 2001, **148**, C376.

57 J. L. Fransaer and R. M. Penner, *J. Phys. Chem. B*, 1999, **103**, 7643–7653.

58 M. Trias and E. Vilaseca, *J. Electroanal. Chem.*, 2004, **569**, 95–109.

59 T. O. Drews, A. Radisic, J. Erlebacher, R. D. Braatz, P. C. Searson and R. C. Alkire, *J. Electrochem. Soc.*, 2006, **153**, C434.

60 T. O. Drews, D. Richard, D. Braatz and C. A. Richard, *Z. Phys. Chem.*, 2007, **221**, 1287–1305.

61 W. Schmickler, K. Pötting and M. Mariscal, *Chem. Phys.*, 2006, **320**, 149–154.

62 M. Mariscal, E. Leiva, K. Pötting and W. Schmickler, *Appl. Phys. A*, 2007, **87**, 385–389.

63 M. H. Mamme, E. A. Mernissi Cherigui, O. Dolgikh, J. Ustarroz, H. Simillion, H. Terryn and J. Deconinck, *Electrochim. Acta*, 2016, **197**, 307–317.

64 M. H. Mamme, J. Deconinck and J. Ustarroz, *Electrochim. Acta*, 2017, **258**, 662–668.

65 O. Dolgikh, A. Bastos, A. Oliveira, C. Dan and J. Deconinck, *Corros. Sci.*, 2016, **102**, 338–347.

66 G. Hills, A. Kaveh Pour and B. Scharifker, *Electrochim. Acta*, 1983, **28**, 891–898.

67 B. Scharifker and G. Hills, *J. Electroanal. Chem. Interfacial Electrochem.*, 1981, **130**, 81–97.

68 A. J. Bard and M. Stratmann, *Encyclopedia of electrochemistry*, Wiley-VCH, vol. 2 edn, 2002.

69 M. Rezaei, S. H. Tabaian and D. F. Haghshenas, *J. Electroanal. Chem.*, 2012, **687**, 95–101.

70 M. Rezaei, S. H. Tabaian and D. F. Haghshenas, *Electrochim. Acta*, 2012, **59**, 360–366.

71 H. Liu and R. Penner, *J. Phys. Chem. B*, 2000, **104**, 9131–9139.

72 J.-C. Bian, Z. Li, Z.-D. Chen, H.-Y. He, X.-W. Zhang, X. Li and G.-R. Han, *Appl. Surf. Sci.*, 2011, **258**, 1831–1835.

73 S. Domínguez-Domínguez, J. Arias-Pardilla, Á. Berenguer-Murcia, E. Morallón and D. Cazorla-Amorós, *J. Appl. Electrochem.*, 2008, **38**, 259–268.

74 Z. Wei, S. Chen, Y. Liu, C. Sun, Z. Shao and P. Shen, *J. Phys. Chem. C*, 2007, **111**, 15456–15463.

75 L. Wang, W. Mao, D. Ni, J. Di, Y. Wu and Y. Tu, *Electrochem. Commun.*, 2008, **10**, 673–676.

76 E. Gómez, R. Pollina and E. Vallés, *J. Electroanal. Chem.*, 1995, **386**, 45–56.

77 H. Harti, J.-L. Bubendorff, A. Florentin, C. Pirri and J. Ebothe, *J. Cryst. Growth*, 2011, **319**, 79–87.

78 K. Hartl, M. Nesselberger, K. J. Mayrhofer, S. Kunz, F. F. Schweinberger, G. Kwon, M. Hanzlik, U. Heiz and M. Arenz, *Electrochim. Acta*, 2010, **56**, 810–816.

79 M. Giesen, *Prog. Surf. Sci.*, 2001, **68**, 1–153.

80 C. Bréchignac, P. Cahuzac, F. Carlier, M. de Frutos, A. Masson, C. Mory, C. Colliex and B. Yoon, *Phys. Rev. B: Condens. Matter Mater. Phys.*, 1998, **57**, R2084–R2087.

81 E. Seebauer, *Prog. Surf. Sci.*, 1995, **49**, 265–330.

82 R. Alayan, L. Arnaud, M. Broyer, E. Cottancin, J. Lermé, S. Marhaba, J. L. Vialle and M. Pellarin, *Phys. Rev. B: Condens. Matter Mater. Phys.*, 2007, **76**, 075424.

83 B. Geboes, J. Ustarroz, K. Sentosun, H. Vanrompay, A. Hubin, S. Bals and T. Breugelmans, *ACS Catal.*, 2016, **6**, 5856–5864.

84 H. E. M. Hussein, H. Amari and J. V. Macpherson, *ACS Catal.*, 2017, **7**, 7388–7398.

85 J. Mostany, J. Mozota and B. Scharifker, *J. Electroanal. Chem. Interfacial Electrochem.*, 1984, **177**, 25–37.

86 J. Mostany, J. Parra and B. R. Scharifker, *J. Appl. Electrochem.*, 1986, **16**, 333–338.

87 W. Simons, D. Gonnissen and A. Hubin, *J. Electroanal. Chem.*, 1997, **433**, 141–151.

88 A. O. Simm, X. Ji, C. E. Banks, M. E. Hyde and R. G. Compton, *ChemPhysChem*, 2006, **7**, 704–709.

89 J. Ustarroz, A. Hubin and H. Terryn, in *Handbook of Nanoelectrochemistry: Electrochemical Synthesis Methods, Properties, and Characterization Techniques*, 2016.

90 L. Komsiyska and G. Staikov, *Electrochim. Acta*, 2008, **54**, 168–172.

91 T. Le Manh, E. Arce-Estrada, M. Romero-Romo, I. Mejía-Caballero, J. Aldana-González and M. Palomar-Pardavé, *J. Electrochem. Soc.*, 2017, **164**, D694–D699.

92 E. A. Mernissi Cherigui, K. Sentosun, P. Bouckenooge, H. Vanrompay, S. Bals, H. Terryn and J. Ustarroz, *J. Phys. Chem. C*, 2017, **121**, 9337–9347.